



Power Electronic Systems  
Laboratory

© 2011 IEEE

Proceedings of the IEEE Energy Conversion Congress and Exposition (ECCE USA 2011), Phoenix, USA,  
September 18-22, 2011.

## **Rotor Position Measurement for a Magnetically Levitated 500'000 rpm Permanent Magnet Machine**

C. Zingerli  
P. Imoberdorf  
T. Nussbaumer  
J.W. Kolar

This material is posted here with permission of the IEEE. Such permission of the IEEE does not in any way imply IEEE endorsement of any of ETH Zurich's products or services. Internal or personal use of this material is permitted. However, permission to reprint/republish this material for advertising or promotional purposes or for creating new collective works for resale or redistribution must be obtained from the IEEE by writing to [pubs-permissions@ieee.org](mailto:pubs-permissions@ieee.org). By choosing to view this document, you agree to all provisions of the copyright laws protecting it.



Eidgenössische Technische Hochschule Zürich  
Swiss Federal Institute of Technology Zurich

# Rotor Position Measurement for a Magnetically Levitated 500'000 rpm Permanent Magnet Machine

Claudius M. Zingerli, Philipp Imoberdorf and Johann W. Kolar  
Power Electronic Systems Laboratory  
ETH Zurich  
8092 Zurich, Switzerland  
Email: zingerli@lem.ee.ethz.ch

Thomas Nussbaumer  
Levitronix GmbH  
Technoparkstr. 1  
8005 Zurich, Switzerland  
Email: nussbaumer@levitronix.com

**Abstract**—In this paper, we propose a DSP or FPGA based transversal flux eddy current sensor position measurement technique for rotors in high-speed electrical drives using active magnetic bearings. Compared to the state-of-the-art demodulation technique using analog mixers or rectifiers, the published method shows a lower circuit complexity and allows fulfilling the high bandwidth needs of highly dynamic systems as well as the improved accuracy necessary in precision bearings. Accordingly and also verified by experiments, the concept is well suited to measure the rotor position of a developed ultra-high-speed electrical drive.

**Index Terms**—Position measurement, Magnetic levitation, Digital control, Digital filters, Modeling, Eddy currents

## I. INTRODUCTION

Research in ultra-high-speed and high-power-density electrical drives has achieved speeds of up to 1 Mrpm [1]. By increasing the rotational speed at a constant output power, the size of a drive can be reduced. Therefore, in conformity with the general trend in power electronics towards smaller dimensions, more compact drives can be used in applications as turbocompressors, air-to-power systems, micro gas turbines, drills and milling spindles [2–4].

At high speeds, the bearings are a critical component of the drive system often dominating losses and limiting the lifetime of the system [5]. Active magnetic bearings (AMBs) offer various advantages at high rotational speeds, there being no contact between rotor and stator and therefore neither wear nor friction. At ETH Zurich a magnetic bearing for such an ultra-high-speed drive system is currently under development [2].

The performance of AMBs depends on the measurement of the rotor's position. There are AMBs that need no explicit position sensors - so called sensor-less bearings - which observe the rotor position by its influence on the bearing coils [6, 7], but most state-of-the-art AMBs still use distinct position sensors usually based on optical, capacitive, inductive or eddy current effects. To facilitate commissioning and because of the weak magnetic feedback of the rotor to the bearing, none of the sensor-less bearing methods are applicable to the system in [2]. Therefore, an explicit position sensor has to be employed.

Eddy current effect based position sensors allow a compact design, need no or only few active components and are comparatively insensitive to EMI which was why they were used. The small dimensions and corresponding high dynamics of the system require a fast detection of the rotor position. To achieve a target speed of 500 krpm (8.33 kHz), several bending modes of the rotor have to be passed through where the position sensor needs to be able to detect the rotor's position.

The goal of this paper is to demonstrate both the feasibility of an eddy current sensor-based radial position measurement system based on direct digital demodulation and filtering, with a bandwidth sufficient to detect rotor displacements up to the rated speed of 500 krpm, and to achieve a precision which lies significantly below the bearings air gap of 200  $\mu\text{m}$ .

In section II the used eddy current based transversal flux sensor is explained. Techniques to amplify the sensor's weak signals are studied in the following section III. Sections IV, V and VI cover the digital demodulation and filtering including an adaptive phase control necessary in harsh environments or long cables. Finally, results from the experimental setup described in section VII are published in section VIII.

## II. TRANSVERSAL FLUX SENSOR

Compared to standard eddy current sensors, the transversal flux sensor (TFS) solely consists of a PCB, so no magnetic cores, windings and coil mounts are needed.

Supplied with an excitation voltage or current, it generates a magnetic field in the excitation coil concentric to the rotor and returns a voltage induced in two anti-serial connected sensor coils for each axis radially placed on opposite sides of the rotor as shown in Fig. 1. It is basically a transformer with a variable coupling and therefore can be modeled using the circuit shown in Fig. 2. This model has been developed in [8] by using PEEC method based GeckoEMC analysis tools. The necessary excitation frequency has to be set in order to fulfill the following requirements:

- Ability to detect position deviations at rotational speed.
- Achievement of maximal mutual coupling of the excitation and sensor coils defined by the sensor layout.

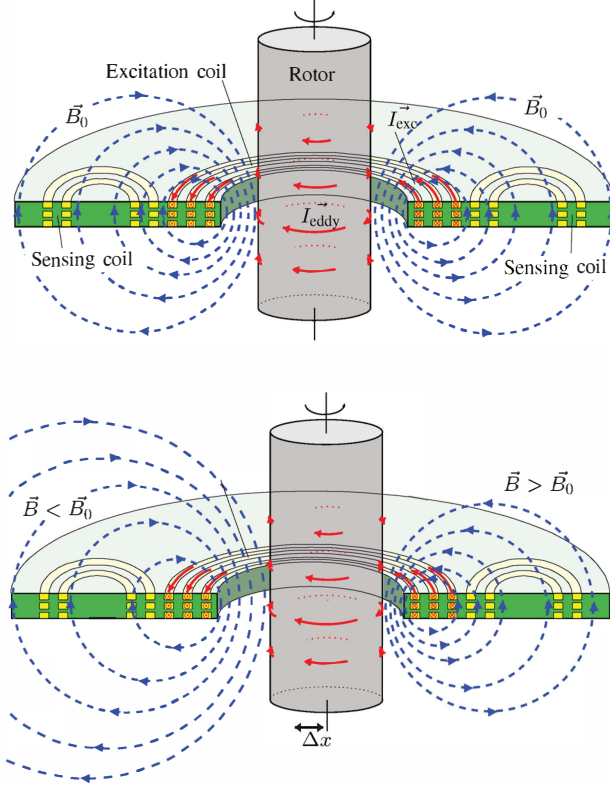


Fig. 1: Layout of a transversal flux sensor with field lines (dashed, blue) with a centered rotor (top) and a displaced rotor by  $\Delta x$  (bottom) according to [8].

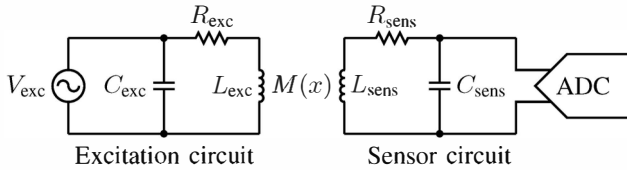


Fig. 2: Equivalent circuit of a transversal flux sensor. Resonant capacitors  $C_{\text{exc}}$  and  $C_{\text{sens}}$  have already been added. The mutual coupling inductance  $M(x)$  depends on the rotor's position  $x$ .

As the magnetic bearing is of a homopolar type, the required bandwidth for bearing control is not essentially as high as the rotational speed. But to be able to observe resonances and rotor orbits at rotational speeds of up to 500 krpm, the position sensor needs to possess a bandwidth of 83.33 kHz when sampling at ten measurements per rotation.

Due to the small rotor diameter at the sensor of about 3 mm, according to [8], the sensor shows the maximum sensitivity at excitation frequencies between 500 kHz and 8 MHz, so both requirements can be satisfied. The used design is specified in Table I.

The first configuration implemented the circuit in Fig. 2 using cables between the sensor and the board containing the excitation source and analog-to-digital-converters (ADCs).

TABLE I: Parameters of the used TFS. Frequency dependent parameters are given at the excitation frequency  $f_{\text{exc}}$ .

Parameter	Value
Sensor inner diameter	3.75 mm
Sensor outer diameter	13.50 mm
Excitation frequency $f_{\text{exc}}$	4.00 MHz
Mutual inductance $M(x)$	7.00 nH/mm
Primary inductance $L_{\text{exc}}$	0.61 $\mu\text{H}$
Primary winding resistance $R_{\text{exc}}$	1.05 $\Omega$
Primary quality factor $Q_{\text{exc}}$	14.6
Secondary inductance $L_{\text{sens}}$	2.12 $\mu\text{H}$
Secondary winding resistance $R_{\text{sens}}$	3.55 $\Omega$
Secondary quality factor $Q_{\text{sens}}$	19.0

This has shown to be very sensitive to coupled noise from the excitation, motor and bearing because of the high impedance of the resonant circuit. Beyond that, to control four axes of a bearing, six resonant circuits needed to be tuned to the same excitation frequency. This together with the weak coupling (7 nH/mm versus the main inductance of 2.12  $\mu\text{H}$ ) made it very difficult to sample at the optimum time. The only advantage of this configuration is that no active components are needed at the bearing which might be advantageous in some applications like high temperature, or radiation environments.

To overcome these disadvantages, a second configuration was developed. The capacitor parallel to the sensing coil was replaced by an +32 dB amplifier with a fourth order bandpass, both on the sensor board. Signals were transmitted to the ADC using current sourced differential connections. This circuit reduced coupled noise, but because of the missing resonant capacitor, the sensing coil started oscillating at diverse eigenfrequencies.

To further eliminate noise coupling, in a third configuration, the resonant capacitor was installed again, together with the excitation source and ADCs moved to the sensor board, leaving a fully digital connection to the control board using six differential pairs.

Other options include downconverting the sensor signals to DC using a mixer and transmitting the low pass filtered signal to the control board. This allows using common DSP integrated ADCs, but limits the bandwidth of the system.

In systems with a bigger rotor diameter, larger sensors with lower excitation frequencies could be used allowing direct demodulation using microcontroller or DSP integrated ADCs.

### III. RESONANT CIRCUIT

In the first and third configuration, a capacitor  $C_{\text{sens}}$  was added in parallel to the sensor coils  $L_{\text{sens}}$  to form a resonant

circuit. This was done to achieve a better suppression of frequencies other than the excitation frequency as well as increase the signal amplitude. Without  $C_{\text{sens}}$ , oscillations at eigenfrequencies of the sensor print were observed. Adding another capacitor  $C_{\text{exc}}$  in parallel or in series to the excitation coil compensates for the coil's reactive power and therefore reduces the load on the excitation amplifier.

The extra gain at the resonance frequency  $f_{\text{res}}$  is equal to the quality factor of the sensor circuit, thus for the given design tuned to  $f_{\text{res}} = 4 \text{ MHz}$  with  $C_{\text{sens}} = 750 \text{ pF}$ ,

$$Q_{\text{sens}} = \frac{\omega_{\text{res}} \cdot L_{\text{sens}}}{R_{\text{sens}}} = \frac{1}{R_{\text{sens}}} \cdot \sqrt{\frac{L_{\text{sens}}}{C_{\text{sens}}}} = +23.2 \text{ dB} \quad (1)$$

are gained without adding any active elements. This comes at the cost of a high source impedance of

$$Z_{\text{sens}}(f_{\text{exc}}) = \frac{Z_0^2}{R_{\text{sens}}} - j \cdot Z_0 \approx 1.01 \text{ k}\Omega \quad , \quad (2)$$

which adds an error if the ADC's input impedance is low and no buffer amplifier is used.

The excitation frequency could be chosen to be below, at or above the resonance frequency. Common eddy current sensors are usually operated besides the resonance frequency keep the phase and gain relatively constant. The resulting losses in signal amplitude from these operation points are not acceptable in our TFS, as due to the small dimensions, coupling and signals are already very small. Therefore the sensor is operated at the resonance frequency  $f_{\text{res}}$ , where the signal gain is maximal, but the resulting phase is also most sensitive to parameter changes. Parameters influencing the phase include part tolerances, temperature dependency of copper resistance  $R_{\text{sens}}$  or capacitor  $C_{\text{sens}}$ . The phase sensitivity - group delay - at resonance is with a value of

$$\frac{d\varphi}{d\omega} = \frac{2 \cdot L_{\text{sens}}}{R_{\text{sens}}} \approx 17.2^\circ / 1\% \text{ deviation of } f_{\text{res}} \quad , \quad (3)$$

quite high why a phase tracking solution has to be considered.

#### IV. SAMPLING AND DEMODULATION

The sensor's output signal is sampled and converted to a digital signal. At first, equal sampling and excitation frequencies are assumed:  $f_{\text{samp}} = f_{\text{exc}}$ .

To achieve maximum sensitivity it's necessary to sample at the amplitude peak. Because the phase difference between excitation and sampling is variable, the optimal sampling phase has to be detected during initial calibration by varying the sampling phase and keeping the maximum. Doing so, it's possible to correct sign errors by sampling at  $180^\circ$  instead of  $0^\circ$ .

If several axes (i.e. two radial axes) are sampled at the same time, often an optimal solution isn't possible because the resonant circuits are not tuned to exactly the same frequency and therefore result in a different phase at a specific frequency.

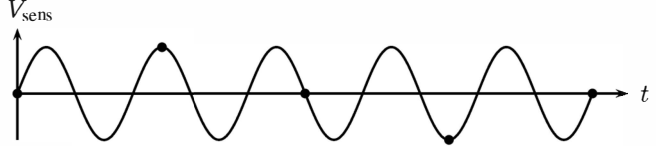


Fig. 3: Sampling at  $f_{\text{samp}} = \frac{4}{5} \cdot f_{\text{exc}}$  with sampling instances indicated by dots.

TABLE II: Different sampling frequencies  $f_{\text{samp}}$  to detect phase and avoid DC signals. Resolution gain is defined as signal gain times frequency gain relative to synchronous sampling at  $f_{\text{samp}} = 4 \text{ MHz}$ .

Samples/Period	$f_{\text{samp}}$	Phase detect	DC separable	Resolution gain
4/1	16 MHz	+	+	+6.02 dB
3/1	12 MHz	+	+	+4.77 dB
2/1	8 MHz	-	+	+6.02 dB
4/3	5.3 MHz	+	-	-3.52 dB
1/1	4.0 MHz	-	-	0 dB
4/5	3.2 MHz	+	+	-7.96 dB
2/3	2.6 MHz	-	+	-3.52 dB
4/7	2.3 MHz	+	+	-10.88 dB

#### V. PHASE OPTIMIZATION

After an initial calibration, aging and heating changes component parameters. Therefore the sensor's phase delay  $\Delta\varphi = \varphi_{\text{sens}} - \varphi_{\text{exc}}$  also changes during operation. As said before, to achieve maximum position sensitivity, sampling should occur at the peak amplitude. To detect any DC component (for example generated by injecting a bias current to measure the wiring's temperature as proposed in [9] or for early detection of sensor failure by monitoring its impedance) as well as common-mode errors from the ADC, the signal should not only be sampled at the positive peak, but also at the negative peak. This assumes that the mechanical bandwidth is significantly below the excitation frequency.

It's easiest to detect the signal's phase when sampling at  $0^\circ$  and  $180^\circ$  as if the phase error is smaller than  $\pm \frac{\pi}{2}$  the difference between the two samples is approximately proportional to the phase. Table II shows common variants for sampling the signal. Other variants are also possible (like for example Samples/Period=3/2), but need different gains for each sample. The trivial implementation uses synchronous sampling with equal excitation frequency  $f_{\text{exc}}$  and sampling frequency  $f_{\text{samp}}$ , but then, neither the phase nor common-mode signals can be detected.

Being able to choose any arbitrary phase further allows to compensate for runtime delays which is necessary when using long cables as at  $f_{\text{exc}} = 4 \text{ MHz}$  the phase delay  $\Delta\varphi$  is about  $14^\circ$  per meter. If there were no compensation, after about six

meters, the signal would have a phase delay of  $90^\circ$  making it impossible to detect using p.e. a synchronous rectifier.

Sampling at  $f_{\text{samp}}/f_{\text{exc}} = 3.2 \text{ MHz}/4 \text{ MHz} = 4/5$  as shown in Fig. 3 allows detection of phase and DC offset. The sampling frequency is close to the excitation frequency, but compared to synchronous sampling at  $f_{\text{samp}}/f_{\text{exc}} = 1$  the resolution is decreased when only evaluating two of four samples as signal amplitude.

## VI. FILTERING

The ADCs output signals are filtered using an FPGA and then transferred to the DSP feeding the position controller. Filtering is done to reduce sensor noise, limit the signal bandwidth to the controller's frequency as well as to increase the resolution. As filter, an integrating moving average filter with reduced complexity shown in Fig. 4 has been used because of its linear response and efficient implementation. The transfer function of the filter is

$$G_{\text{filter}}(z) = \frac{1 - z^{-n}}{1 - z^{-1}} \quad (4)$$

with  $n$  equal to the number of delays and therefore zeroes at multiples of  $\frac{2 \cdot \pi \cdot f_{\text{samp}}}{n+1}$ . This structure can be derived from the traditional FIR approach of a moving average filter with a transfer function of

$$G_{\text{FIR}}(z) = 1 + z^{-1} + z^{-2} \dots + z^{-m} \quad (5)$$

which basically is a geometric series. By calculating the  $m$ -th partial sum defined as

$$s_m := \sum_{k=0}^m q^k = \frac{1 - q^{m+1}}{1 - q} \Big|_{|q| \neq 1}, \quad (6)$$

substituting  $q$  by  $z^{-1}$  and excluding the last element, the transfer function of the implemented filter in (4) results when defining

$$m := n - 1. \quad (7)$$

The number of registers grows linearly in both implementations, but the number of adders is constant equal to two in the used model, while in the traditional FIR approach it's proportional to  $n$ . The excluded last element of the traditional FIR approach has been moved to the integrator in Fig. 4. Even though the feedback structure suggests the possibility to be destabilizable, it's not as the internal loop gain is equal to one. Compared to the traditional FIR approach, it needs an initial reset (which can e.g. be used to correct offset errors of the sensors/ADCs) and is not safe against random bit flips.

This structure can further be transformed into a one-stage zero-delay decimating CIC filter, published 1981 by Hogenauer [10]. The sum in Fig. 4 is split into an adder for the integrator and a subtractor for the delay chain. As the system is linear, the integrator can be put before the delay chain and instead of delaying the samples by  $n$  clocks, the clock frequency is decreased to  $1/n$  and a sampling element is added in between the two parts, so the delay chain becomes a differentiator (called

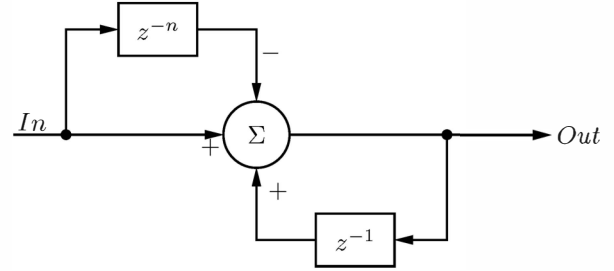


Fig. 4: Implemented moving average filter requiring  $n + 1$  delays, one subtractor and one adder.

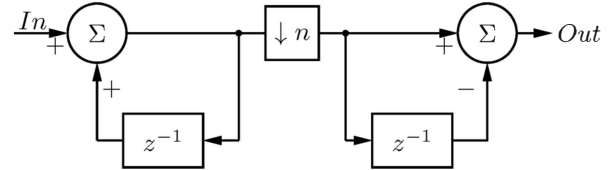


Fig. 5: Transformation into a CIC filter structure.

*comb stage* in [10]) running at  $1/n$  the input clock frequency as shown in Fig. 5. The filter's gain of  $n$  is understood as a change of base (unity in the position controller's system equals  $n$  times unity in the ADC's system) and therefore there is no attenuation necessary.

## VII. EXPERIMENTAL SETUP

In order to test the proposed methods, several experiments were conducted. Figures 6, 7 and 8 show the developed control electronics and different versions of the position sensor.

The excitation signals are generated using a Class-E amplifier on the control board for the sensor shown in Fig. 7 or directly on the sensor board as shown in Fig. 8. Clocking and tuning for the excitation and sampling is done in the FPGA. The logic allows frequency and phase changes under operation in steps of  $2^\circ$  at  $f_{\text{samp}} = 4 \text{ MHz}$ . The sensor in Fig. 7 is - besides the optional digital temperature sensor - passive. This comes at the cost of delicate cabling - noise is easily coupled into the sensor signals. As ADCs, 40 Msps, 10 bit ADCs with integrated preamps from TI were used. In later experiments, the excitation and ADC circuits were moved to the sensor boards, where 3.5 Msps, 14 bit-ADCs with SPI and LVDS interfaces from Linear Technology were chosen. Cable coupled noise was eliminated, but the complexity of the sensor increased.

## VIII. MEASUREMENTS

The sensor's bode plot is shown in Fig. 9. The influence of a resonance capacitor parallel to the sensing coil is clearly visible (Tagged *with*  $C_{\text{sens}}$ ). The capacitor adds less gain and less phase shift than expected: At resonance, only  $+18.1 \text{ dB}$  are gained at the expense of  $125^\circ$  phase delay. The group

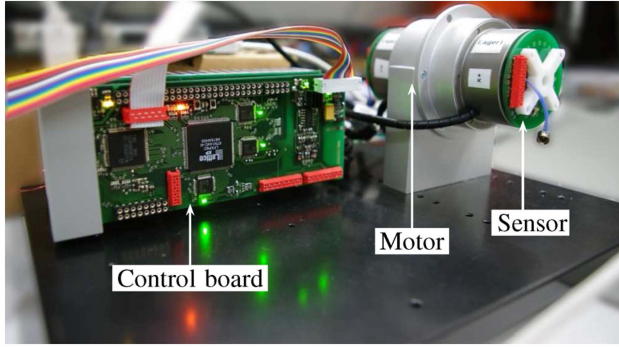


Fig. 6: Complete magnetically levitated system. The left part is the control board consisting of a DSP for force and position control as well as an FPGA for position sensing and filtering. Behind the control board five full bridge inverters are mounted on a heat sink to supply the bearing. On the right, the magnetically levitated 500 krpm motor with discussed position sensors on both sides can be seen. The motor and bearing have been designed by [2].

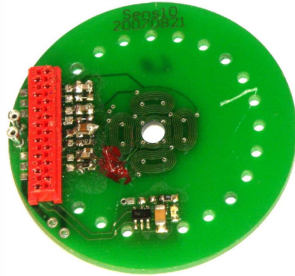
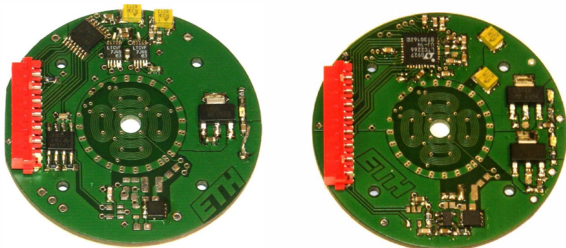


Fig. 7: Passive sensor consisting only of excitation and sensor coils and corresponding capacitors. A digital temperature sensor has been added to observe the sensor's temperature. Excitation signal generation and sampling is done on the control board.



(a) Low-end ADC allowing subsynchronous sampling up to 3.5MSPS (b) Fast ADC allowing oversampling

Fig. 8: Two variants of active sensors with integrated excitation and digitalization. Both use completely digital, differential serial busses to the control system what eliminated coupled noise.

delay (phase change per frequency change) at the resonance frequency increased from  $-8^\circ/\text{MHz}$  without capacitor to  $-204^\circ/\text{MHz} = -8.2^\circ/1\%f_{\text{exc}}$  with capacitor.

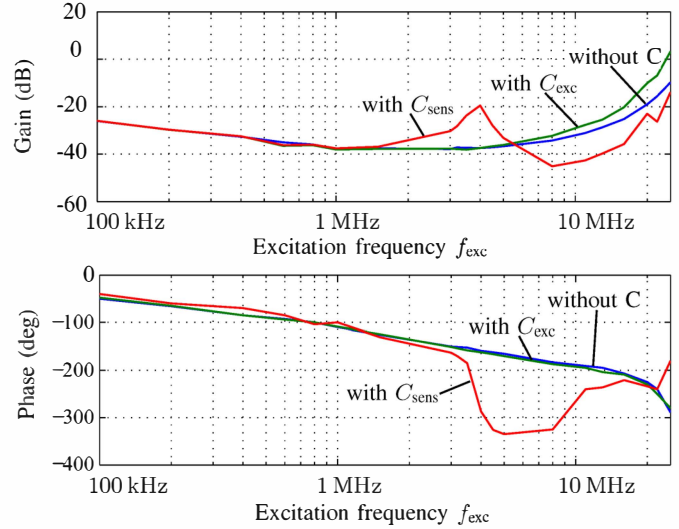


Fig. 9: Sensor voltage transfer function for different configurations with and without resonant capacitors. Compared to the configurations without  $C_{\text{sens}}$ , the sensor gain (top) increases by 18.1 dB at resonance using a capacitor  $C_{\text{sens}}$  parallel to the sensor coil, but the phase sensitivity (bottom) changes as well from  $0.32^\circ/1\%f_{\text{exc}}$  to more than  $8.2^\circ/1\%f_{\text{exc}}$  when using  $C_{\text{sens}}$ .

Results above  $f_{\text{exc}} = 10 \text{ MHz}$  are questionable and might come from the measurement setup. Keeping the excitation amplifier's impedance constant, at higher frequencies the excitation voltage increases what amplifies the influence of parasitic capacitances. By adding a 1 pF, 3 k $\Omega$  RC-circuit in between of the excitation and sensing coils, a similar effect could be achieved in simulation.

One sensor PCB always measures two axes. The output voltage of the two axes of a sensor is shown in Fig. 10. At the center ( $x = y = 0 \mu\text{m}$ ), the signals change their sign which corresponds to a phase shift of  $180^\circ$ . The rotor bore is not perfectly centered why the two axes have different limits. Even though the rotor bore is very close to the innermost winding of the excitation coil, nonlinearity is very limited.

To test the independence of the two channels of the sensor ( $x$  and  $y$ ), a grid with a mesh size of  $50 \mu\text{m}$  was measured. The results are shown in Fig. 11. The black circle characterizes the limitation of the rotor's displacement in the real system with installed touchdown bearings.

The influence of the length of the filter in the FPGA is shown in Table III and Fig. 12. A sampling frequency equal to the excitation frequency was used to collect the data in the table and figure. With increasing length of the filter, the output frequency drops and the position resolution increases. The standard deviation of the measured position  $\sigma_x$  diminishes as well. The comparatively large noise at short filter lengths of  $n = 1$  and  $n = 2$  is based on the big value of the least significant bit (LSB) in these cases.

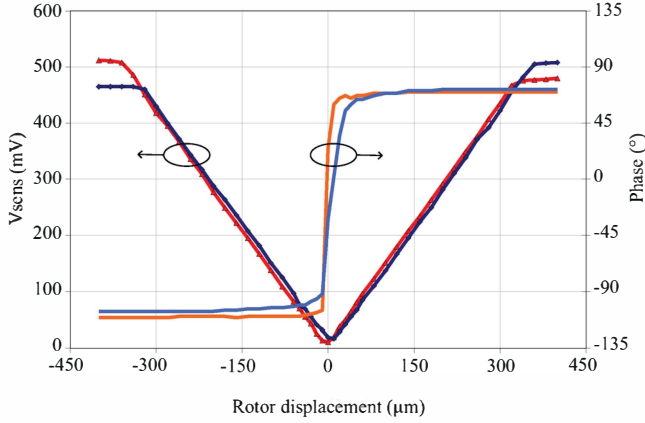


Fig. 10: Axis independence and linearity. The gain of the two sensor axes per TFS is equal the outputs a linear function of the rotor displacement.

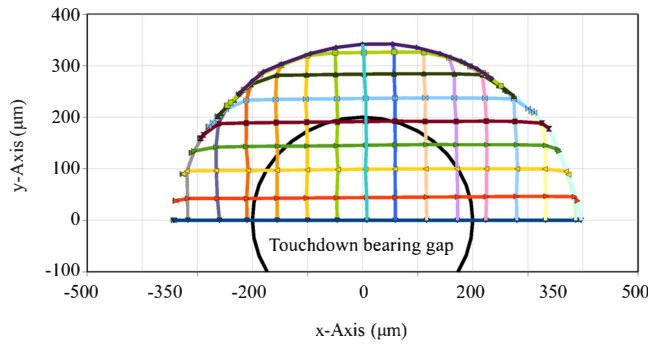


Fig. 11: Measured mesh. The rotor has been moved along a grid of  $50 \mu\text{m}$  and the sensor's signals were traced. The black circle shows the limitation of the rotor's displacement with touchdown bearings in place.

A filter length of  $n = 16$  was selected because it has the best suppression of noise, highest resolution and frequency components of the bearing controller's frequency of  $200 \text{ kHz}$  are still in the pass band.

## IX. CONCLUSIONS

In this paper, a completely digital position sensing system for active magnetic bearings was presented. It proved to be reliable and flexible in the experiment. It replaces the Eurocard-sized analog system and allows for an integration of the position sensing electronics on the bearing controller board.

Thanks to the achievable resolution in the micrometer range at bandwidths in the megahertz range it is particularly well suited for very high speed position measurement. Further applications may include monitoring of piezo crystals, ultrasonic or interferometry.

Currently (May 2011), the magnetically levitated motor used for the testing of the published position sensing system reaches

TABLE III: Comparison of position noise at different filter lengths  $n$

Length $n$	1	4	16	64	256
Res. [bit]	10	12	14	16	18
$f_0$ [kHz]	4000	1000	250	62.5	15.6
$\mu\text{V}/\text{LSB}$	1953	488	122	31.5	7.6
$\sigma_{\text{LSB}}$ [LSB]	0.47	0.93	2.07	4.61	13.2
$\sigma_v$ [ $\mu\text{V}$ ]	918	454	253	141	101
$\sigma_x$ [nm]	656	325	181	101	71.8

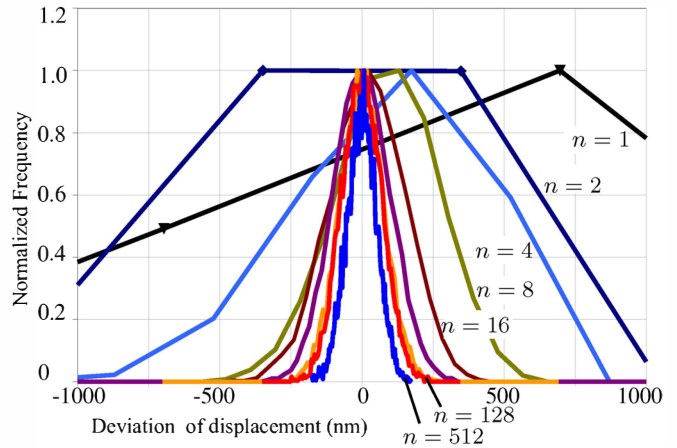


Fig. 12: Histogram of position noise at different filter lengths  $n$ .

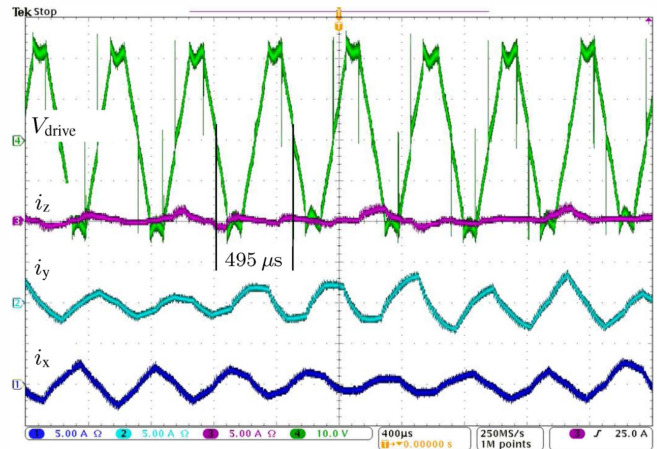


Fig. 13: Bearing currents of the motor at a speed of  $121 \text{ krpm}$ .  $i_x$ ,  $i_y$  and  $i_z$  are the bearing currents and  $V_{\text{drive}}$  is the motor voltage.

a speed of  $121 \text{ krpm} = 2.02 \text{ kHz}$  as shown in Fig. 13. At this speed, rotor unbalance becomes a major problem. For future experiments, the rotor needs to be overworked in order to reduce unbalance.

## REFERENCES

- [1] J. W. Kolar, S. D. Round, and C. Zwyssig, "Megasppeed drive systems: Pushing beyond 1 million r/min," *IEEE/ASME Trans. Mechatronics*, vol. 14, no. 5, pp. 564–574, Oct 2009.
- [2] P. Imoberdorf, C. Zwyssig, S. D. Round, and J. W. Kolar, "Combined radial-axial magnetic bearing for a 1 kw, 500,000 rpm permanent magnet machine," in *Applied Power Electronics Conference, APEC 2007*, Mar 2007, pp. 1434–1440.
- [3] D. Krähenbühl, C. Zwyssig, H. Weser, and J. W. Kolar, "A miniature, 500 000 rpm, electrically driven turbocompressor," in *Proc. IEEE Energy Conversion Congress and Exposition ECCE*, 2009, pp. 3602–3608.
- [4] C. Zwyssig, J. Kolar, W. Thaler, and M. Vohrer, "Design of a 100 w, 500000 rpm permanent-magnet generator for mesoscale gas turbines," in *Industry Applications Conference, 2005. Fourtieth IAS Annual Meeting*, vol. 1, Oct. 2005, pp. 253 – 260 Vol. 1.
- [5] D. Krähenbühl, C. Zwyssig, H. Weser, and J. Kolar, "Mesoscale electric power generation from pressurized gas flow," in *Proc. Power MEMS, 2008*, Nov. 2008, pp. 377 – 380.
- [6] D. Vischer and H. Bleuler, "Self-sensing active magnetic levitation," *IEEE Trans. Magn.*, vol. 29, no. 2, pp. 1276 –1281, Mar. 1993.
- [7] T. Tera, Y. Yamauchi, A. Chiba, T. Fukao, and M. Rahman, "Performances of bearingless and sensorless induction motor drive based on mutual inductances and rotor displacements estimation," *IEEE Trans. Ind. Electron.*, vol. 53, no. 1, pp. 187 – 194, Feb. 2005.
- [8] A. Müsing, C. Zingerli, P. Imoberdorf, and J. W. Kolar, "PEEC-based numerical optimization of compact radial position sensors for active magnetic bearings," in *5th International Conference on Integrated Power Electronics Systems*, 2008.
- [9] L. Burdet, "Active magnetic bearing design and characterization for high temperature applications," Ph.D. dissertation, Ecole Polytechnique Federale de Lausanne, Sep 2006.
- [10] E. Hogenauer, "An economical class of digital filters for decimation and interpolation," *IEEE Trans. Acoust., Speech, Signal Process.*, vol. 29, no. 2, pp. 155 – 162, Apr. 1981.